

# Amphiphilic Zwitterionic Bioderived Block Copolymers from Glutamic Acid and Cholesterol – Ability to Form Nanoparticles and Serve as Vectors for the Delivery of 6-Mercaptopurine

Meike N. Leiske,\* Christopher Kuenneth, Jonas De Breuck, Bruno G. De Geest, and Richard Hoogenboom\*

In this work, the straightforward synthesis of amphiphilic zwitterionic bioderived block copolymers (BCPs) using glutamic acid (Glu) and cholesterol (Chol) as building blocks are reported. The previously established Glu-derivative NBoc-Glu-OtBu-methacrylate (NBoc-Glu-OtBu-MA) serves as hydrophobic precursor for the zwitterionic block, while a mostly unexplored cholesteryl-derived methacrylate monomer (Chol-MA) with increased side chain flexibility functions as the hydrophobic block. In the first step, NBoc-Glu-OtBu-MA is polymerized via reversible addition-fragmentation chain-transfer (RAFT) polymerization. Afterward, the linear polymer is chain-extended with Chol-MA, yielding  $P(\text{NBoc-Glu-OtBu-MA})_n\text{-}b\text{-(Chol-MA)}_m$  BCPs with varying block ratios. After deprotection under acidic conditions, polymers with a block weight ratio of 87:13 (Glu-OH-MA:Chol-MA) readily assemble into polymeric nanoparticles (NPs) of a desirable size below 100 nm diameter, making them good candidates for biomedical applications. The experimental results are supported using computations of the partition coefficients and machine learning models for the prediction of the polymer densities of the different BCPs. In addition, high (up to 20 wt.%) loading of the hydrophobic anti-cancer drug 6-mercaptopurine (6-MP) is achieved in these NPs during the assembly process. The cytostatic activity of 6-MP NPs is demonstrated in vitro on MDA-MB-231 breast cancer cells. These results emphasize the potential of amphiphilic zwitterionic bioderived NPs for the delivery of hydrophobic drugs.


## 1. Introduction

During the last decades, polymer nanomedicine has received rising attention.<sup>[1]</sup> Synthetic polymers were used for drug delivery platforms in different ways: i) polymer nanoparticles (NPs), ii) stimuli-responsive polymer-drug conjugates, or iii) therapeutic polymers.<sup>[2]</sup> The use of polymers is rapidly emerging, and conjugation of drugs can help to improve their solubility,<sup>[3]</sup> blood circulation time,<sup>[4]</sup> and tissue distribution,<sup>[5]</sup> which leads to a reduction of interaction with nontumor cells and limit toxic side effects.

Hydrophilic non-ionic polymers such as poly(ethylene glycol) (PEG),<sup>[6]</sup> poly(cyclic imino ether)s,<sup>[7]</sup> and poly(2-hydroxypropylmethacrylamide)<sup>[8]</sup> exhibit low protein adsorption and prolonged blood circulation time, and, therefore, have gained interest to suppress unwanted interactions with proteins and cells.<sup>[9]</sup> While low fouling properties are advantageous to decrease unwanted cellular interactions, they can also reduce the association with the target tissue and cells, which is known as the PEG dilemma.<sup>[9b, 10]</sup> Interestingly,

M. N. Leiske, J. De Breuck  
 Faculty of Biology  
 Chemistry & Earth Sciences  
 University of Bayreuth  
 Universitätsstraße 30, 95447 Bayreuth, Germany  
 E-mail: meike.leiske@uni-bayreuth.de

M. N. Leiske  
 Bavarian Polymer Institute  
 Universitätsstraße 30, 95447 Bayreuth, Germany  
 M. N. Leiske, R. Hoogenboom  
 Supramolecular Chemistry Group  
 Centre of Macromolecular Chemistry (CMaC)  
 Department of Organic and Macromolecular Chemistry  
 Ghent University  
 Krijgslaan 281 S4, Ghent B-9000, Belgium  
 E-mail: richard.hoogenboom@ugent.be  
 C. Kuenneth  
 Faculty of Engineering Science  
 University of Bayreuth  
 Universitätsstraße 30, 95447 Bayreuth, Germany

 The ORCID identification number(s) for the author(s) of this article can be found under <https://doi.org/10.1002/macp.202300200>

© 2023 The Authors. Macromolecular Chemistry and Physics published by Wiley-VCH GmbH. This is an open access article under the terms of the Creative Commons Attribution License, which permits use, distribution and reproduction in any medium, provided the original work is properly cited.

DOI: 10.1002/macp.202300200

zwitterionic polymers, can combine low fouling characteristics<sup>[11,12]</sup> while showing specific uptake by cancer cells in vitro and accumulation in solid tumors in vivo.<sup>[13,14]</sup> Previously, most studies have focused on polybetaines (i.e., carboxybetaines, sulfobetaines, or phosphobetaines).<sup>[12a, 15]</sup> It is assumed that surface proteins, such as amino acid transporters – which are sometimes referred to as zwitterion transporters – contribute to this specificity.<sup>[14a]</sup> Recently, Sakurai and co-workers reported on the affinity of polycarboxybetaine bottle brushes to zwitterionic transporters on the cell surface.<sup>[14b]</sup> More recently, amino-acid-derived zwitterionic polymers were reported to show an even stronger affinity to cancer cells compared to polybetaines.<sup>[16]</sup> The contribution of amino acid transporters to the specific uptake of  $\alpha$ -amino-acid-functionalized polymers was demonstrated by different groups.<sup>[14b, 16-17]</sup> In addition, their chemical versatility allows an effortless manipulation of the polymer structure. We have previously shown that modifications to the polymer backbone can be exploited to tailor the properties and cell specificity of glutamic acid (Glu)-derived polyzwitterions.<sup>[17b]</sup> Glu-functionalized polymethacrylates showed the highest specificity to MDA-MB-231 breast cancer cells. One advantage of the previously developed Glu-derived systems is the hydrophobic character of the NBoc-Glu-OtBu making the derived polymers accessible for chain-extension with hydrophobic monomers due to solubility in similar solvents. In contrast, zwitterionic polybetaines are predominantly polymerized in aqueous media.<sup>[15]</sup> Cholesterol, which is an important component of the lipid double layer of cells,<sup>[18]</sup> is an established component for the formulation of stable liposomes including the COVID-19 vaccines.<sup>[19]</sup> Previously, cholesterol-methacrylate monomers were successfully prepared by reacting the hydroxyl group of cholesterol with methacryloyl chloride.<sup>[20]</sup> The polymerization of the resulting cholesteryl methacrylate mostly resulted in oligomers,<sup>[21]</sup> potentially caused by steric hindrance and solubility issues. To the best of our knowledge, the preparation of amphiphilic block copolymers (BCPs) consisting of a hydrophobic cholesterol-derived block and a hydrophilic, zwitterionic block has not been reported to date. However, it seems an attractive strategy for the development of bioderived drug delivery vectors for hydrophobic drugs.

6-mercaptopurine (6-MP), a thiol-containing nucleobase adenine and guanine analog, is an anticancer drug. As antimetabolite, it can be incorporated into DNA and, consequently, interferes with DNA production and cell division.<sup>[22]</sup> To date, 6-MP is used for the treatment of lymphoblastic leukemia and lymphoblastic lymphoma,<sup>[23]</sup> however, its therapeutic efficacy is hampered by its low bioavailability, short blood circulation times, and various side effects (e.g., diarrhea, nausea, vomiting, loss of appetite, or fatigue). To improve its performance, its insolubility in aqueous systems and unwanted absorption to serum proteins must be overcome.<sup>[24]</sup> Previously, efforts have been made to improve the drug's performance by the conjugation to polyethyleneglycol (PEG)<sup>[25]</sup> or encapsulation into chitosan NPs.<sup>[24b]</sup> To the best

of our knowledge, the encapsulation of 6-MP into amphiphilic zwitterionic polymeric transporters has not been reported.

Previously, we studied the synthesis and polymerization of different vinylic Glu-derivatives and demonstrated specific interaction of these polymers with cancer cells, compared to non-cancerous cells, in vitro.<sup>[17b]</sup> Polymers made from a Glu-derived methacrylate (P(Glu-OH-MA)) featured controlled polymerization, low side-chain hydrolysis, and high cellular specificity. Hence, we decided to use P(Glu-OH-MA) as a hydrophilic block for the design of amphiphilic BCPs comprising cholesterol motifs in the hydrophobic block. The synthesis of cholesteryl methacrylates from cholesterol and methacryloyl chloride has been previously reported.<sup>[20]</sup> However, solution polymerization of this monomer remains challenging and often leads to oligomers instead.<sup>[21]</sup> Therefore, we elaborated on a different approach in the current study, aiming to design a vinylic cholesteryl monomer, which can be (block co-)polymerized in solution in a controlled manner.

The work in this study is supported by polymer informatics approaches. Past efforts in the field of polymer informatics have demonstrated the capacity of data-driven machine-learning techniques to expedite discovery, design, development, and deployment of polymeric materials.<sup>[26]</sup> These techniques leverage experimental and computational data to make predictions in unexplored parts of the polymer chemical space and guide subsequent experimentation.<sup>[27]</sup> The computation of the partition coefficients and prediction of the polymer densities (using the predictors of the Polymer Genome project),<sup>[28]</sup> which is done in this work, is an example of the extensive capabilities and potentialities encompassed by polymer informatics.

Here we developed nanocarriers based on BCPs composed of a hydrophobic, cholesterol-derived block and a hydrophilic zwitterionic glutamic-acid-derived block. Therefore, we chose a mostly unexplored cholesteryl methacrylate (Chol-MA) with enhanced side chain flexibility and synthesized polymers via reversible addition-fragmentation chain-transfer (RAFT) chain-extension polymerization. To this end, we first polymerized NBoc-Glu-OtBu via RAFT polymerization as previously established, resulting in monomodal distributed homopolymers, which could be chain-extended with Chol-MA. After deprotection, the zwitterionic, amphiphilic BCPs were assembled into polymeric NPs. We also computed the partition coefficient<sup>[27b,29]</sup> and use the Polymer Genome<sup>[28]</sup> framework to predict density and volume fractions of each block in the BCPs. We applied the BCPs for the encapsulation of 6-MP and evaluated their cytostatic activity in vitro on MDA-MB-231 breast cancer cells.

## 2. Results and Discussion

### 2.1. Synthesis and Characterization

In the first step, the Chol-MA monomer was synthesized. Previously, this monomer has been synthesized from cholesterol and 2-methacryloyloxyethyl isocyanate.<sup>[30]</sup> In this study, we decided to react aminoethyl methacrylate hydrochloride and cholesteryl chloroformate (Scheme S1, Supporting Information) instead to form the carbamate bond. The formation of Chol-MA from aminoethyl methacrylate and cholesteryl chloroformate was verified via <sup>1</sup>H NMR analysis of the purified monomer (**Figure 1A**),

B. G. De Geest  
Department of Pharmaceutics and Cancer Research Institute Ghent (CRIG)  
Ghent University  
Ottergemsesteenweg 460, Ghent B-9000, Belgium

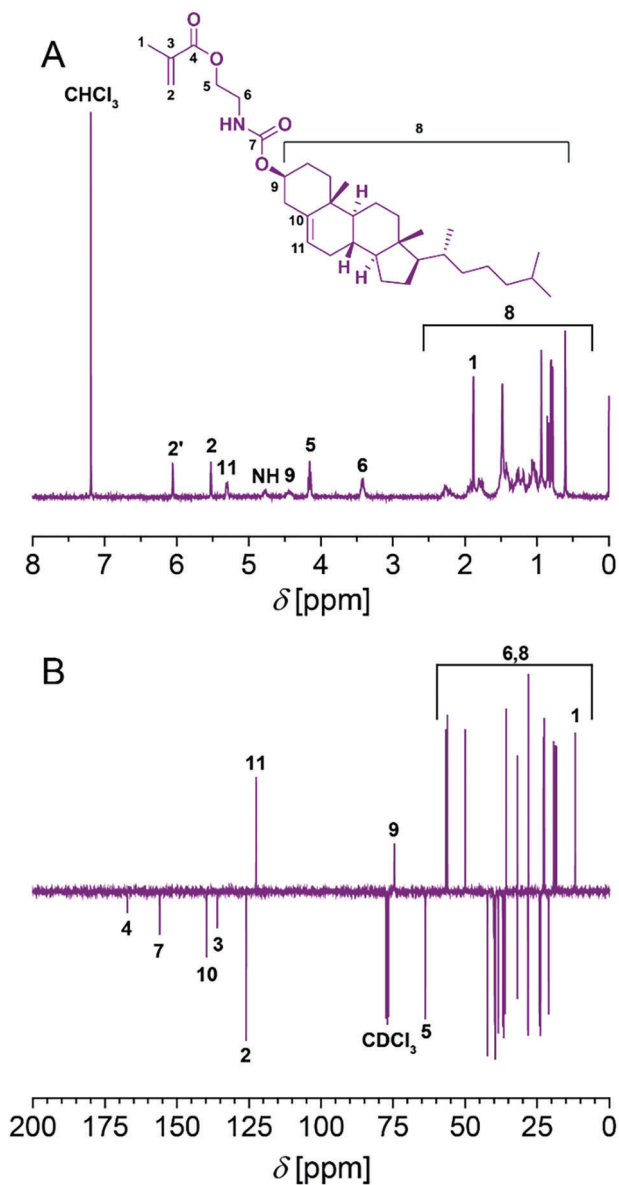


**Figure 1.** Characterization of Chol-MA. A: <sup>1</sup>H NMR spectrum (300 MHz, CDCl<sub>3</sub>). B: <sup>13</sup>C (DEPT) NMR spectrum (75 MHz, CDCl<sub>3</sub>).

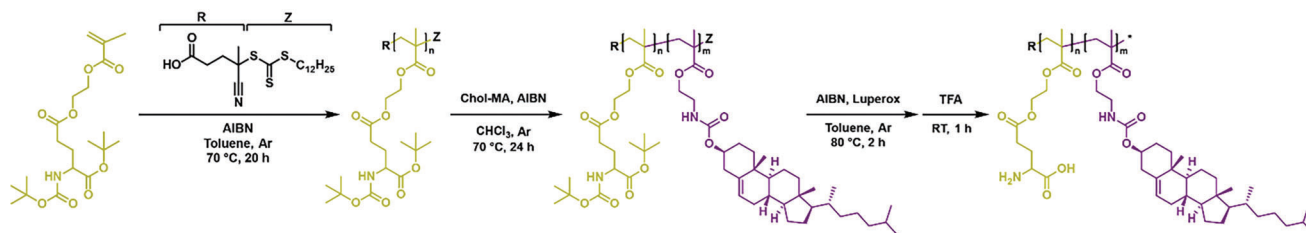
showing the appearance of the typical vinyl signals at  $\delta = 6.06$  (H<sub>2</sub>) and  $\delta = 5.54$  (H<sub>2'</sub>) ppm. The appearance of the NH-peak at  $\delta = 4.80$  ppm indicated the successful formation of the carbamate bond during the reaction. In addition, <sup>13</sup>C NMR spectroscopy (Figure 1B) confirmed the success of the reaction by a downfield shift of the corresponding carbonyl carbon (C7) to  $\delta = 156.1$  ppm.

BCPs were prepared via RAFT polymerization using a monomer (M) to chain-transfer agent (CTA) ([M]/[CTA]) ratio of 150:1 with 4-cyano-4-[(dodecylsulfanylthiocarbonyl)sulfanyl]pentanoic acid (CDTA) as CTA based on our earlier reports on the polymerization of NBoc-Glu-O*t*Bu-MA.<sup>[17b]</sup> This Glu-derived monomer features a Boc-protecting group on its amine functionality as well as a *t*Bu-group protecting the  $\alpha$ -carboxylic acid, while its  $\gamma$ -carboxylic acid was used for the esterification with hydrox-

ethyl methacrylate. After 20 h, a near quantitative monomer conversion (> 95%) was confirmed by the absence of vinyl groups in the <sup>1</sup>H NMR spectrum, yielding P(NBoc-Glu-O*t*Bu-MA)<sub>140</sub>-CTA. After purification, the obtained macro-CTA was chain-extended with Chol-MA at different [M]/[CTA] ratios (i.e., 20:1, 50:1, 75:1). Due to the limited solubility of Chol-MA in toluene and dimethylsulfoxide (DMSO), chloroform was chosen as a reaction solvent for the chain-extension reaction (Scheme 1).

All block copolymerization reactions reached conversions of 50 – 65% of Chol-MA, yielding a small series of BCPs. Excessive Chol-MA was removed by precipitation of the polymer in ice-cold *n*-hexane. The molar mass distribution of the different polymers was analyzed by size-exclusion chromatography (SEC) on three different systems using N,N-dimethylformamide (DMF), tetrahydrofuran (THF), and CHCl<sub>3</sub> as eluents (Table 1 and Table S1, Supporting Information Figures 2 and 4). Notably, these solvents have been reported earlier as suitable solvents for cholesterol derivatives.<sup>[31]</sup> Compared to the Glu-derived homopolymer P(NBoc-Glu-O*t*Bu-MA)<sub>140</sub>, a negligible shift of the peak maximum to lower retention times was observed in DMF, even for P(NBoc-Glu-O*t*Bu-MA)<sub>140</sub>-*b*-P(Chol-MA)<sub>40</sub> (Figure S3A, Supporting Information). We attribute this to a collapse of the BCPs in DMF, which was also indicated by the observed stagnation of the number-average molar mass ( $M_n$ ) and dispersity ( $\mathcal{D}$ ) (Table 1) as well as other indicators (i.e., asymmetry factor ( $A_s$ ), skewness ( $\alpha_3$ ), and kurtosis ( $\alpha_4$ )), calculated from the SEC measurements (Table S2, Supporting Information).<sup>[32]</sup> Similar results were obtained when using THF as an eluent (Figure 2B). Only SEC analysis using CHCl<sub>3</sub> as an eluent revealed an obvious shift of the elugrams of BCPs to lower retention times compared to the Glu-derived homopolymer (Figure 2C). (Table 2)

Deprotection of the Boc groups by previously established conditions,<sup>[17b]</sup> yielded P(Glu-OH-MA)<sub>140</sub>-*b*-P(Chol-MA)<sub>m</sub> BCPs. Due to the limited solubility of P(Glu-OH-MA)<sub>140</sub> and P(Glu-OH-MA)<sub>140</sub>-*b*-P(Chol-MA)<sub>10</sub> in organic solvents, they were analyzed via thermogravimetric analysis (TGA; Figure S4, Supporting Information). We observed that the polymers degraded in different stages. The first stage of mass loss (90 °C) was associated with the loss of water.<sup>[33]</sup> After that, P(Glu-OH-MA)<sub>140</sub> decomposed in four stages: i) 100 °C – 190 °C (24 wt.% mass loss), ii) 190 °C – 258 °C (18 wt.% mass loss), iii) 258 °C – 348 °C (14 wt.% mass loss), and iv) 348 °C – 500 °C (23 wt.% mass loss). The first stage was presumably associated with the decarboxylation of the free acid in the side chain akin to poly(acrylic acid),<sup>[34]</sup> while the second degradation step was likely caused by anhydride formation.<sup>[35]</sup> During the third decomposition stage, ester bonds were cleaved, which has been previously also shown for cationic amino-acid-derived polymethacrylates.<sup>[36]</sup> The fourth region indicated the degradation of the polymeric backbone.<sup>[37]</sup> In case of P(Glu-OH-MA)<sub>140</sub>-*b*-P(Chol-MA)<sub>10</sub> a similar degradation profile was observed, however showing weight losses of i) 15, ii) 13, iii) 19, and iv) 29 wt.%, respectively. The differences were attributed to the cleavage of carbamate bonds during the third stage of decomposition<sup>[38]</sup> as well as the degradation of cholesterol within during the fourth region,<sup>[39]</sup> indicating the presence of Chol-MA in the deprotected BCP. In addition, Fourier-transform infrared spectroscopy (FTIR) measurements confirmed the presence of cholesterol units (Figure S5, Supporting Information) by the bands observed at  $\nu \sim 3390, 2775 - 3000, 1634, \text{ and } 1360$



**Scheme 1.** Synthesis of amphiphilic BCPs featuring a hydrophilic Glu-OH-MA block and a hydrophobic Chol-MA block. For simplification purposes, Glu-OH-MA is shown in its non-ionic form.

**Table 1.** Characterization of polymers.

Polymer	mol% NBoc-Glu-OtBu-MA <sup>a)</sup>	mol% Chol-MA <sup>b)</sup>	$M_n$ <sup>b)</sup> [kg mol <sup>-1</sup> ]	$\mathcal{D}$ <sup>b)</sup>	$M_n$ <sup>c)</sup> [kg mol <sup>-1</sup> ]	$\mathcal{D}$ <sup>c)</sup>	$M_n$ <sup>d)</sup> [kg mol <sup>-1</sup> ]	$\mathcal{D}$ <sup>d)</sup>
P(NBoc-Glu-OtBu-MA) <sub>140</sub>	100	0	20.9	1.38	30.3	1.22	37.5	1.28
P(NBoc-Glu-OtBu-MA) <sub>140</sub> - <i>b</i> -P(Chol-MA) <sub>10</sub>	93	7	23.3	1.31	30.1	1.30	34.2	1.37
P(NBoc-Glu-OtBu-MA) <sub>140</sub> - <i>b</i> -P(Chol-MA) <sub>31</sub>	82	18	25.1	1.24	31.0	1.25	39.6	1.27
P(NBoc-Glu-OtBu-MA) <sub>140</sub> - <i>b</i> -P(Chol-MA) <sub>40</sub>	78	22	23.8	1.51	33.8	1.20	39.5	1.27

<sup>a)</sup> Calculated from monomer conversion obtained from <sup>1</sup>H NMR (300 MHz) in CDCl<sub>3</sub>; <sup>b)</sup> SEC in CHCl<sub>3</sub>; polystyrene (PS)-calibration; <sup>c)</sup> SEC in THF; PS-calibration; <sup>d)</sup> SEC in DMF supplemented with LiBr (5 g L<sup>-1</sup>); PS-calibration.

cm<sup>-1</sup>, corresponding to Chol-MA. FTIR further confirmed the purity from trifluoroacetic acid by the absence of its characteristic bands at  $\nu^- = 3250$  and 1790 cm<sup>-1</sup>.

## 2.2. 6-Mercaptopurine-loaded NPs

NPs were prepared from deprotected BCPs, via the thin-film assembly technique<sup>[40]</sup> (Scheme 2). Dynamic light-scattering (DLS) analysis indicated that, out of the three tested polymers, only P(Glu-OH-MA)<sub>140</sub>-*b*-P(Chol-MA)<sub>10</sub> formed NPs (Figures S6 and S7, Supporting Information). For this reason, all further experiments were conducted with P(Glu-OH-MA)<sub>140</sub>-*b*-P(Chol-MA)<sub>10</sub>.

To further understand the assembly of the designed amphiphilic BCPs, we used machine learning models of the Poly-

mer Genome project<sup>[27b, 28]</sup> to predict the densities (Figure 3A) and volume fractions (Figure 3B) of the block copolymers.

The predictions showed larger block densities with increasing degree of polymerisation (DP) content as reported elsewhere.<sup>[41]</sup> The densities of the relevant repeating units were predicted to i)  $\rho = 1.6$  g cm<sup>-3</sup> for P(Glu-OH-MA)<sub>140</sub> and ii)  $\rho = 1.05$  to 1.11 g cm<sup>-3</sup> for P(Chol-MA)<sub>10</sub> to P(Chol-MA)<sub>30</sub>. Based on these values, the relative volume fractions of the zwitterionic hydrophilic Glu-OH-MA block and the hydrophobic Chol-MA block were calculated. We found an increase in the volume fraction of the hydrophobic block from 18 to 43% with increasing Chol-MA content. Previous studies reported that amphiphilic BCPs with hydrophobic blocks of up to 50% volume fractions could form micellar, spherical NPs.<sup>[42]</sup> However, in our case, only the BCP with 18% Chol-MA volume fraction formed spherical micelles. To solve this, it was assumed that the longer Chol-MA block prevents

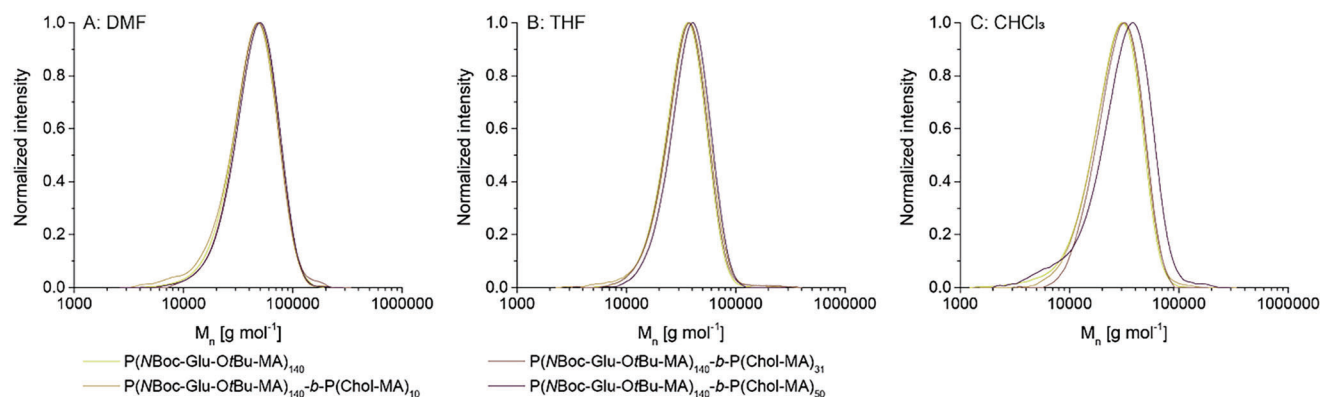


**Figure 2.** Characterization of the molar mass distribution of P(NBoc-Glu-OtBu-MA)<sub>140</sub> homopolymer and chain-extended P(NBoc-Glu-OtBu-MA)<sub>140</sub>-*b*-P(Chol-MA)<sub>m</sub> BCPs. Polymers were synthesized via RAFT polymerization. A) SEC measurements in DMF. Molar mass distribution obtained from PS calibration. B) SEC measurements in THF. Molar mass distribution obtained from PS calibration. C) SEC measurements in CHCl<sub>3</sub>. Molar mass distribution obtained from PS calibration. For elugrams see Figure S3 (Supporting Information).

**Table 2.** Molar and weight ratios of Glu-OH-MA and Chol-MA repeating units in different BCPs as determined (see Table 1).

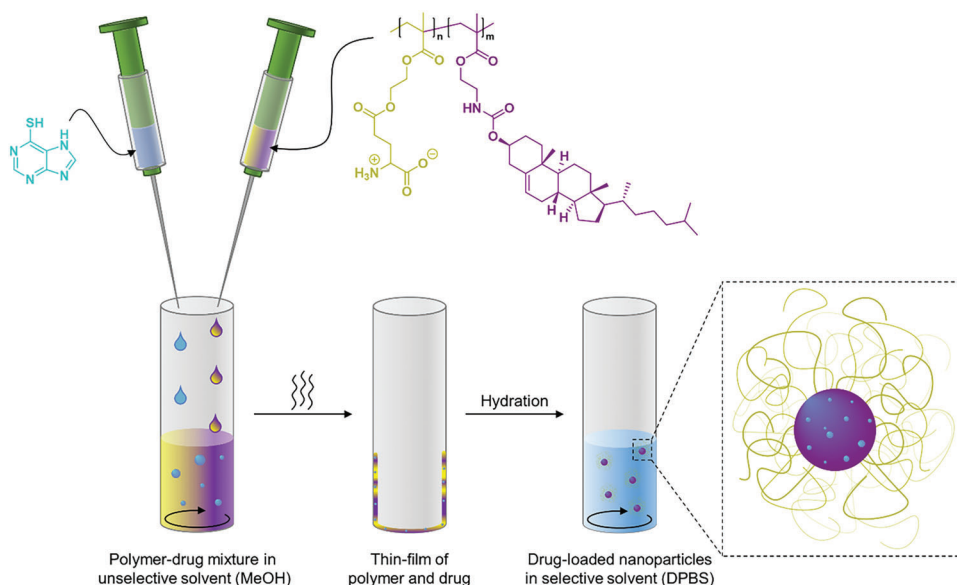
Polymer	mol% <sup>a)</sup> Glu-OH-MA	mol% <sup>a)</sup> Chol-MA	wt.% <sup>a)</sup> Glu-OH-MA	wt.% <sup>a)</sup> Chol-MA	V <sub>f</sub> <sup>b)</sup> (Chol-MA) [%]	Log p <sup>c)</sup> [a.u.]
P(Glu-OH-MA) <sub>140</sub>	100	0	100	0	0	-155.42
P(Glu-OH-MA) <sub>140</sub> - <i>b</i> -P(Chol-MA) <sub>10</sub>	93	7	87	13	18	-144.28
P(Glu-OH-MA) <sub>140</sub> - <i>b</i> -P(Chol-MA) <sub>31</sub>	82	18	69	31	40	-147.87
P(Glu-OH-MA) <sub>140</sub> - <i>b</i> -P(Chol-MA) <sub>40</sub>	78	22	63	37	46	-149.88

n.a. not available <sup>a)</sup> determined from <sup>1</sup>H NMR conversion of the monomers after RAFT polymerization; <sup>b)</sup> computed from the density predictions from the Polymer Genome project; <sup>c)</sup> computed using RDKit.

the micellar-forming process because of increased hydrophobicity that can be determined using the partition coefficient of the blocks. Due to the demanding chemistry and solvability of the amphiphilic zwitterionic polymers, standard experimental analyses of the partition coefficient were not conducted. Instead, we computed the partition coefficient of the block copolymers using the cheminformatics tool RDKit<sup>[43]</sup> which implements the method described by Wildman and Crippen<sup>[29]</sup> (Figure 3C, D). Interestingly, we found that BCPs with ten units of Chol-MA possessed the highest theoretical partition coefficient ( $\log p = -145.5$  a.u.) and hydrophobicity respectively, while the addition of more Chol-MA units led to a decrease of  $\log p$ , indicating a more hydrophilic character of the BCP despite the longer hydrophobic blocks of 31 or 40 repeating units of Chol-MA. We attributed this behavior to the hydrophilic groups in the side chain of Chol-MA, thereby emphasizing the importance and interplay of all components of the chemical structure of a polymer. This computational finding matches our experiments that only BCP with 18% Chol-MA forms spherical micelles and, therefore, the combination of the increased volume fraction and hydrophilicity of Chol-MA block of longer DPs are unfavorable for self-assembly of the

presented BCPs. Furthermore, these computations highlight the potential of harnessing synergies between experiments and theory, and the pivotal role of data-driven machine learning models in the design and development of polymeric materials and systems.

Owing to its ability to form NPs in aqueous medium, P(Glu-OH-MA)<sub>140</sub>-*b*-P(Chol-MA)<sub>10</sub> was selected for the encapsulation of 6-MP into NPs. To this end, 6-MP was dissolved together with the polymer before thin-film formation, followed by the same procedure as empty described above for the formation of empty NPs. Importantly, NP solutions were absent of aggregates, suggesting the successful encapsulation of 6-MP into polymer NPs. DLS analysis (Figure 4, Figure S7, Supporting Information) showed monomodal size distributions for NPs with a theoretical drug-loading up to 15wt.%, a z-average of 75 to 80 nm in diameter, and a rather narrow polydispersity index (PDI) of 0.2 to 0.3 (Table S2, Supporting Information). NPs with 20 wt.% of 6-MP were slightly bigger (z-average =  $90 \pm 20$  nm), and, although monomodal, also featured slightly more variation in size. Consequently, all NP formulations were found suitable for further in vitro testing.



**Scheme 2.** Depiction of the thin-film assembly of 6-MP (drug) and P(Glu-OH-MA)<sub>n</sub>-*b*-P(Chol-MA)<sub>m</sub> (polymer). Both, the drug, and the polymer are dissolved in an unselective solvent (MeOH) and mixed in a small reaction vial. The vials are shaken at room temperature overnight under continuous airflow to remove the organic solvent and form a thin film on the glass. Upon hydration with a selective solvent (Dulbecco's phosphate buffered saline (DPBS)), drug-loaded NPs are formed.

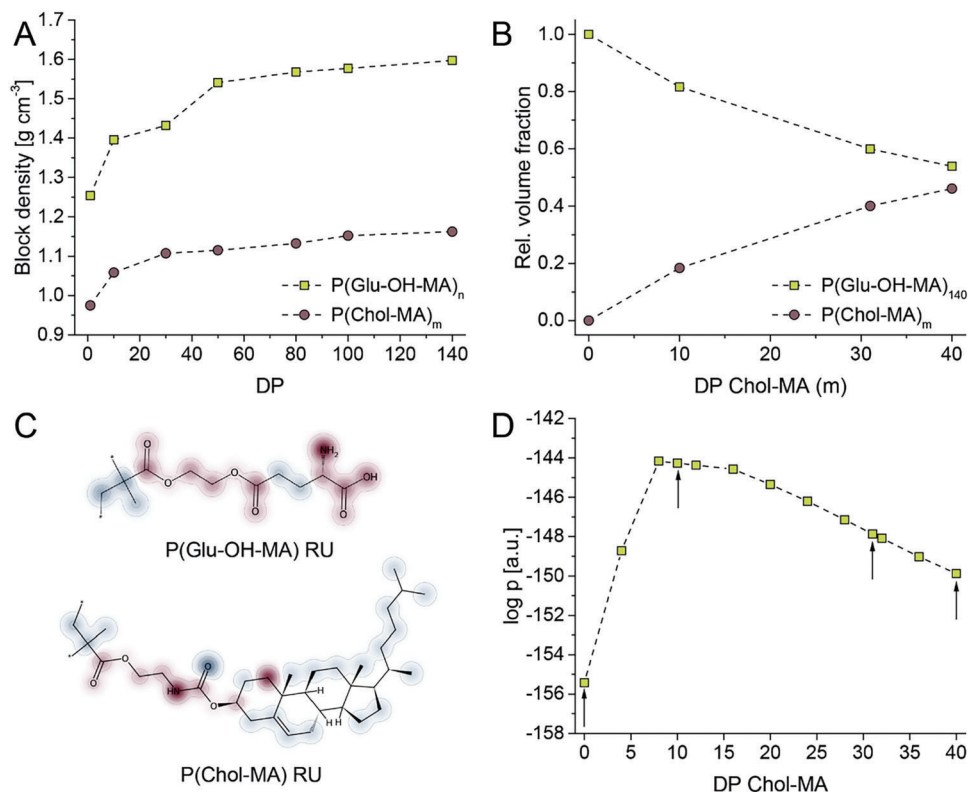


**Figure 3.** Block density, volume fraction, and partition coefficient of block polymers. The block densities were predicted using machine learning models of the Polymer Genome project, volume fractions were computed using the block densities predictions, and the partition coefficients were calculated using the cheminformatics tool RDKit. A) block densities of  $P(\text{Glu-OH-MA})_n$  and  $P(\text{Chol-MA})_m$ . B) volume fractions of  $P(\text{Glu-OH-MA})_{140}$  and  $P(\text{Chol-MA})_m$  of different block copolymers. C) chemical structures of  $P(\text{Glu-OH-MA})$  and  $P(\text{Chol-MA})$  highlighting the hydrophilic (red) and hydrophobic (blue) regions of the structures. The stars in the chemical drawings of panel C indicate the endpoints of the polymer repeat unit. D) Partition coefficients ( $\log p$ ) of different BCPs with  $P(\text{Chol-MA})$  blocks of varying lengths. Arrows indicate the polymers synthesized within this study.

### 2.3. Cytotoxicity

We first tested the cytotoxicity of 6-MP NPs on MDA-MB-231 breast cancer cells using an MTT assay with an incubation time of 24 h (Figure 5; Table S3, Supporting Information). Control NPs without 6-MP did not exhibit acute cytotoxicity (cell viability  $\geq 70\%$ , *cfr.* ISO-10993<sup>[44]</sup>) up to a concentration of  $0.50 \text{ mg mL}^{-1}$ , suggesting their suitability as a drug carrier. In contrast, 6-MP-loaded NPs induced concentration-dependent cytotoxicity on MDA-MB-231 breast cancer cells, showing a significant decrease in viability down to  $61 \pm 6\%$  of the negative control ( $p < 0.0005$ ) at the highest tested concentration ( $0.50 \text{ mg mL}^{-1}$  polymer concentration). Interestingly, the drug loading did not influence the cytotoxic activity of the 6-MP NPs.

Clearly, none of the 6-MP NPs was able to reduce the cell viability below 60%, which suggests a lack of acute cytotoxicity caused by the drugs whose mechanism of action is through interference with cell proliferation and DNA synthesis.<sup>[45]</sup> In fact, unencapsulated 6-MP, added to MDA-MB-231 breast cancer cells from a DMSO stock solution, only reduced the cell viability to a minimum of  $73 \pm 7\%$  ( $p < 0.00005$ ), which further emphasizes the potential resistance of MDA-MB-231 breast cancer cells to 6-MP, which could be facilitated by the expression of multiple drug resistance-associated protein (MRP4) in triple-negative breast cancer cells, such as MDA-MB-231 cells.<sup>[46]</sup>

6-MP NPs were then tested in a three-day in vitro assay to assess their potential to inhibit cell proliferation (Figure 6; Figure S8, Tables S4 and S5, Supporting Information). Empty NPs only slightly affected cell viability, similarly as observed in the 24 h experiment (Figure 5A). In contrast, treatment with 6-MP NPs induced a significant decrease in cell growth ( $p < 0.00005$ ) at all three tested drug loadings (i.e., 5, 10, and 20 wt.% 6-MP; polymer concentration  $0.5 \text{ mg mL}^{-1}$ ; Figure 5A).

In addition, treatment with lower doses of 6-MP NPs (i.e.,  $0.25 \text{ mg mL}^{-1}$ ,  $0.13 \text{ mg mL}^{-1}$ , and  $0.06 \text{ mg mL}^{-1}$ ) revealed an expectedly lower therapeutic effect. Notably, the total cell number did decrease below the starting population after 3 days of treatment, which further highlights the absence of acute cytotoxicity of 6-MP. In fact, as a nucleobase analog, 6-MP interferes with the proliferation of cells, i.e., by being built into the DNA of the new cells which derive from mitosis.<sup>[22,47]</sup> In contrast to DNA intercalating agents such as anthracycline drugs, 6-MP has a limited effect on existing cells but rather prevents them from proliferating.<sup>[48]</sup>

While the results comparing NPs with varying drug loading delivered the expected results of an increased cytostatic effect for NPs with higher drug loading (i.e., 20 wt.%) compared to those with less drug (i.e., 5 wt.%), we were curious about the real benefit of the higher drug loading and thus, also compared formulations with identical drug concentrations and, consequently,

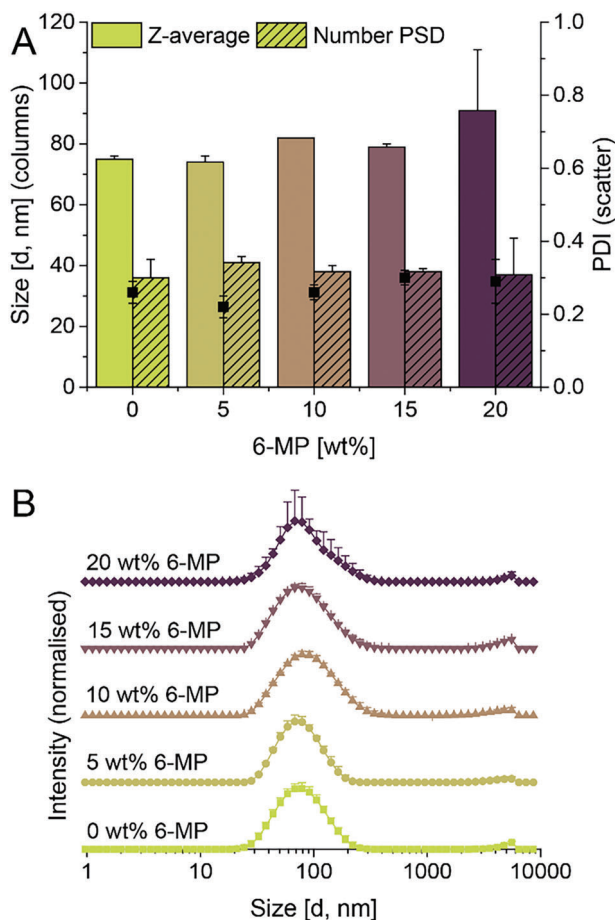


**Figure 4.** Intensity-weighted size-distribution of polymer NPs. NPs were prepared from P(Glu-OH-MA)<sub>140</sub>-*b*-(Chol-MA)<sub>10</sub> and 6-MP at indicated concentrations via thin-film assembly in DPBS at room temperature. NPs were analyzed via DLS measurements at 25 °C (5 measurements with 3 runs each). Weight percentage (wt.%) of 6-MP is relative to polymer mass and assumes 100% drug loading efficiency. Final polymer concentration was 1 mg mL<sup>-1</sup>. A) Size and PDI of NPs shown as mean and standard deviation (SD). B) Normalized intensity distribution traces, shown as mean and SD. For values, refer to Table S2 (Supporting Information).

varying polymer amounts with each other (Figure 6B and C). Cells treated with empty NPs revealed constant proliferation (cell population > 70% compared to the control) independent from the polymer concentration, indicating that the effect of the polymer itself can be neglected. At a drug concentration of 25 μg mL<sup>-1</sup>, NPs with 5 wt.% 6-MP reduced the cell population to 39 ± 2% ( $p < 0.00005$ ), 10 wt.% 6-MP led to a reduction to 42 ± 3% ( $p < 0.00005$ ), and NPs with 20 wt.% had the least effect on the cell population, which was reduced to 56 ± 6% ( $p < 0.005$ ). These results suggest that at the same drug dose, those NPs with lower 6-MP-loading are beneficial to suppress cell proliferation. We assume that the explanation for this phenomenon lies within the number of NPs the cells were treated with. As DLS analysis has shown us that NPs with different drug content are of similar size, it can be concluded that NP solutions if varying 6-MP concentrations contain a similar number of NPs. It is thus concluded that NPs with lower 6-MP-loading already contain enough 6-MP to induce a cytotoxic effect, however, the NPs can reach a larger

number of cells, due to the increased number of NPs present in solution. Detailed studies on the cellular association and internalization of these NPs will be conducted as part of future studies further investigating the versatility of these systems. Our results demonstrate the suitability of NPs made from amphiphilic, bioderived polymers for the delivery of 6-MP. Furthermore, it is emphasized that ultrahigh drug loading is not necessary to induce cytostatic effects in MDA-MB-231 breast cancer cells. Future studies will further explore these interesting BCPs in polymer drug delivery and their potential to form different kinds of assemblies in solution.

### 3. Conclusion

Amphiphilic BCPs consisting of the zwitterionic hydrophilic Glu-derived methacrylate Glu-OH-MA and the hydrophobic cholesterol-derived methacrylate Chol-MA were synthesized. The Glu-derived block was synthesized via RAFT polymerization and subsequently chain-extended with Chol-MA to yield BCPs with different hydrophilic-hydrophobic ratios. BCPs were assembled via thin-film assembly yielding polymer NPs of a diameter of ≈75 nm depending on the computed density and volume fraction of the two blocks, as well as the computed partition coefficient of the respective polymer. NPs consisted of a hydrophobic, cholesterol-derived core and a hydrophilic zwitterionic Glu-derived shell. The hydrophobic anti-cancer drug 6-mercaptopurine could be encapsulated into NP at a drug loading of up to 20 wt.%. 6-MP-loaded NPs induced cytostatic effects on MDA-MB-231 breast cancer cells in vitro while empty NPs were non-toxic. Our current results emphasize the suitability of biomimetic, amino-acid-derived NPs for drug delivery applications.

### 4. Experimental Section

**Materials:** Lauroyl peroxide (Luperox, Acros Organics), toluene (Sigma-Aldrich), ethyl acetate (Sigma-Aldrich), *n*-hexane (Sigma-Aldrich), 2-hydroxyethyl methacrylate (HEMA, TCI), Boc-L-glutamic acid  $\alpha$ -*tert*-butyl ester (Sigma Aldrich), anhydrous dichloromethane (DCM, Sigma-Aldrich), *N,N*-dimethylacetamide (DMAC, HPLC grade, 99.8+%), lithium chloride (LiCl, Fisher Scientific), *N,N*-dicyclohexylcarbodiimide (DCC, Sigma-Aldrich), 4-dimethylamino-pyridine (DMAP, Sigma Aldrich), 4-cyano-4-[(dodecylsulfanylthiocarbonyl)sulfanyl]-pentanoic acid (CDTA, Sigma-Aldrich), Dulbecco's phosphate buffered saline (DPBS, Gibco), fetal bovine serum (FBS, Gibco), Dulbecco's Modified Eagle Medium: Nutrient Mixture F-12 (DMEM/F12, Gibco), Trypsin (Gibco), were used as received. Deionized water was prepared with a resistivity <18.2 MΩ cm using an Arium 611 from Sartorius with the Sartopore 2 150 (0.45 + 0.2 μm pore size) cartridge filter. Azobisisobutyronitrile (AIBN, Sigma-Aldrich) was recrystallized from methanol prior to use. All other chemicals were purchased from standard suppliers and used as received. NBoc-Glu-O $\beta$ Bu-methacrylate (NBoc-Glu-O $\beta$ Bu-MA) was synthesized as previously reported by the group.<sup>[17b]</sup>

**Nuclear Magnetic Resonance (NMR) Spectroscopy:** <sup>1</sup>H and <sup>13</sup>C Distortionless Enhancement by Polarization Transfer (DEPT) Nuclear Magnetic Resonance (NMR) spectroscopy. NMR spectroscopy of all samples was carried out using a Bruker AVANCE III HD 300 MHz or 400 MHz spectrometer as indicated utilizing deuterated solvents obtained from Sigma-Aldrich.

**Size-Exclusion Chromatography (SEC):** SEC was performed on three different systems as indicated to analyze the polymer masses and dispersity.

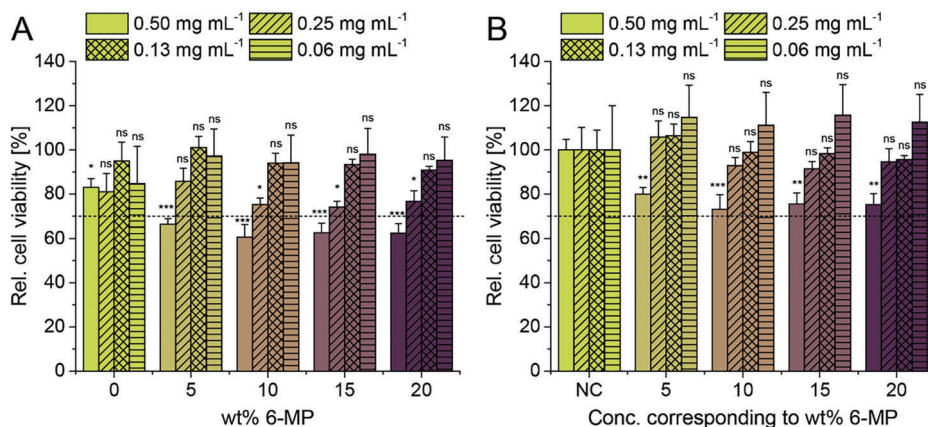


**Figure 5.** Cell viability of MDA-MB-231 breast cancer cells after incubation with A) various NP formulations at indicated concentrations and B) unformulated 6-MP added from DMSO stock solutions for 24 h. Weight percentage (wt.%) of 6-MP is relative to polymer mass and assumes 100% drug loading efficiency. Cell viability was determined by MTT assay. Concentrations in legends refer to polymer concentration in (A) and corresponding polymer concentration in (B). Cells without polymer treatment served as negative control (NC, 100% cell viability). Values shown are relative to the NC. Cells treated with 20% DMSO served as positive control (PC, 0% cell viability, data not shown). In (B), NCs were observed from treatment of cells with DMSO, but in the absence of 6-MP. Statistical significance was analyzed by one-way ANOVA with Tukey's test and represents significance in comparison to the NC. In (B), the corresponding NC with the same concentration of DMSO was compared to the sample. \*\*\* $p < 0.0005$ ; \*\* $p < 0.005$ ; \* $p < 0.05$ ; ns stands for not significant at  $p < 0.05$ . Dashed line represents the threshold for acute cytotoxicity according to ISO-10993-5.<sup>[44]</sup> Mean values and SD can be found in Table S3 (Supporting Information).

**Chloroform system:** The measurements were recorded using an SDV XL gel column (particle size = 5  $\mu\text{m}$  (separation range of 100–3 000 000 Da) and a refractive index detector (1200 series, Agilent Technologies). Chloroform was used as the solvent and eluent with a flow rate of 0.5  $\text{mL min}^{-1}$ . The calibration was performed with a narrowly distributed polystyrene homopolymer (PSS calibration kit). Before measurement, the sample was dissolved in chloroform and filtered with a 0.22  $\mu\text{m}$  polytetrafluoroethylene (PTFE) filter. The injection volume was 20  $\mu\text{L}$ . Toluene served as the internal standard.

**DMF system:** The measurements were recorded using a GRAM 10  $\mu\text{m}$  3000  $\text{\AA}$  gel column (separation range of 5000–5 000 000 Da) and a refractive index detector (1260 Infinity series, Agilent Technologies). DMF supplemented with LiBr (5  $\text{g L}^{-1}$ ) was used as the solvent and eluent with a flow rate of 0.5  $\text{mL min}^{-1}$ . The calibration was performed with a narrowly distributed polystyrene homopolymer (PSS calibration kit). Before measurement, the sample was dissolved in the eluent and filtered with a 0.22  $\mu\text{m}$  polytetrafluoroethylene (PTFE) filter. The injection volume was 20  $\mu\text{L}$ . Toluene served as the internal standard.

**THF system:** The measurements were recorded using an SDV XL gel column (separation range of 1000–1 000 000 Da) and a refractive index detector (1200 series, Agilent Technologies). THF was used as the solvent and eluant with a flow rate of 0.5  $\text{mL min}^{-1}$ . The calibration was performed with a narrowly distributed polystyrene homopolymer (PSS calibration kit). Before measurement, the sample was dissolved in chloroform and filtered with a 0.22  $\mu\text{m}$  polytetrafluoroethylene (PTFE) filter. The injection volume was 20  $\mu\text{L}$ . Toluene served as the internal standard.

**Description of Molecular Weight Distribution (MWD) Shape by Asymmetry Factor ( $A_s$ ), Skewness ( $\alpha_3$ ), and Kurtosis ( $\alpha_4$ ):** The properties of the MWD shape were calculated after a literature procedure.<sup>[49]</sup> A brief description of the applied equations can be found below.

$$A_s = \frac{V_{el\ max} - V_{peak\ max}}{V_{peak\ max} - V_{el\ min}} \quad (1)$$

$A_s$ : Asymmetry factor;  $V_{el\ max}$ : maximum elution volume at 10% peak height;  $V_{el\ min}$ : minimum elution volume at 10% peak height;  $V_{peak\ max}$ : elution volume of peak maximum

$$\alpha_3 = \frac{M_z M_w M_n - 3M_n^2 M_w + 2M_n^3}{(M_w M_n - M_n^2)^2} \quad (2)$$

$\alpha_3$ : Skewness;  $M_n$ : Number average molar mass;  $M_w$ : Weight average molar mass;  $M_z$ : Z average molar mass

$$\alpha_4 = \frac{M_{z+1} M_z M_w M_n - 4M_n^2 M_z M_w + 6M_n^3 M_w - 3M_n^4}{(M_w M_n - M_n^2)^2} \quad (3)$$

$\alpha_4$ : Kurtosis;  $M_n$ : Number average molar mass;  $M_w$ : Weight average molar mass;  $M_z$ : Z average molar mass;  $M_{z+1}$ : Z+1 average molar mass

**Thermogravimetric Analysis (TGA):** Thermogravimetric analysis (TGA) was conducted on a Mettler TGA/DSC3 using a heating rate of 10  $\text{K min}^{-1}$  from 30  $^\circ\text{C}$  to 700  $^\circ\text{C}$  under a nitrogen atmosphere. The polymer samples were placed in an aluminum oxide ceramic crucible. The weight loss was recorded as a function of the temperature.

**Lyophilization:** Lyophilization of samples was conducted using an Alpha 1–2 LDplus freeze-dryer from Martin Christ Gefriertrocknungsanlagen GmbH (Germany).

**Dynamic Light Scattering (DLS):** DLS was measured on a Zetasizer Nano-ZS Malvern apparatus (Malvern Instruments Ltd) using disposable cuvettes. The excitation light source was a He–Ne laser at 633 nm and the intensity of the scattered light was measured at an angle of 173 $^\circ$ . This method measures the rate of intensity fluctuation, and the size of the particles was determined through the Stokes–Einstein equation. The concentration of the polymer solution was 1  $\text{mg mL}^{-1}$  in DPBS in all cases.

**Fourier-Transform Infrared Spectroscopy (FTIR):** IR spectra were recorded from solids on a Perkin Elmer Spectrum 100 FTIR spectrometer in attenuated total reflection (ATR) mode.

**Synthesis of Cholesteryl-Methacrylate (Chol-MA):** In a 500 mL Schlenk flask, 1.33 g aminoethyl methacrylate hydrochloride ( $8.0 \times 10^{-3}$  mol, 1.2 equiv.) was suspended in 100 mL anhydrous DCM under Ar atmosphere. Subsequently, 2.8 mL  $\text{NEt}_3$  ( $20.0 \times 10^{-3}$  mol, 3.0 equiv.) was added to dissolve the starting material. Upon complete solution, the reaction mixture was cooled in an ice bath. In a separate 100 mL Schlenk flask, 3.0 g cholesteryl chloroformate ( $6.7 \times 10^{-3}$  mol, 1.0 equiv.) was dissolved in 50 mL anhydrous DCM under an argon atmosphere. This solution was then transferred into a dropping funnel and added to the reaction mixture dropwise under vigorous stirring. After that, the reaction mixture was stirred at room temperature overnight. The solvent was removed under reduced pressure using a rotary evaporator. After that, the product was recrystallized from chloroform. After drying the solid in a vacuum oven,



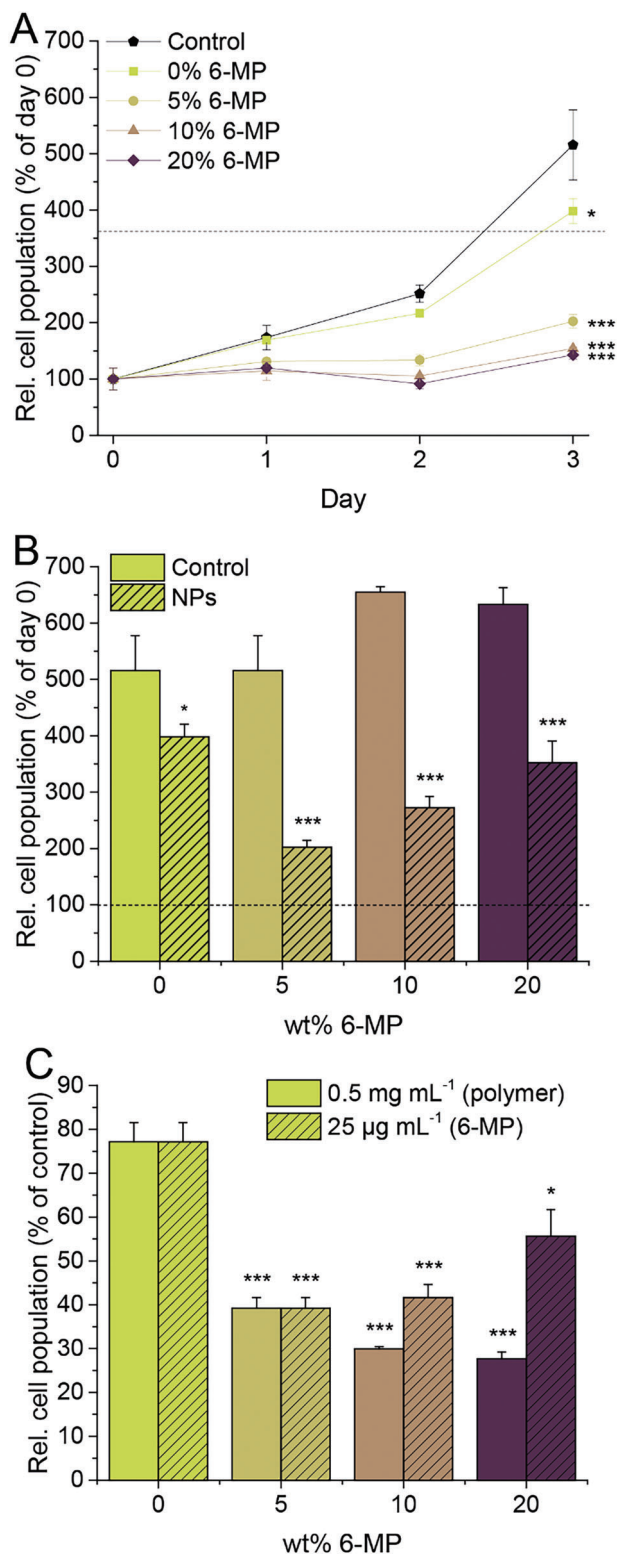


**Figure 6.** Relative in vitro cell growth of MDA-MB-231 breast cancer cells in the presence of drug-loaded polymer NPs. The cells were treated with 100 µL of cell culture media containing 1 mM inhibitor equivalents. Media was changed daily and supplied with compounds as indicated. Cell growth was determined by MTT assay with initial cell seeding of 3000 cells per well. \*\*\* $p < 0.00005$ ; \*\* $p < 0.0005$ ; \* $p < 0.005$ ; ns stands for not significant at  $p < 0.005$ . Significances are relative to control and determined via one-way

the crude product was washed with deionized water using a Büchner funnel and dried in a vacuum oven to obtain the product as a white powder (850 mg, 23%).

<sup>1</sup>H NMR (300 MHz) in CDCl<sub>3</sub>:  $\delta$  = 6.06 (1H, s, CH=C-CO-), 5.54 (1H, s, CH=C-CO-), 5.31 (1H, s, -C=CH-CH<sub>2</sub>- (cholesterol)), 4.80 (0.9H, s, br, -CH<sub>2</sub>-NH-C=O-), 4.44 (1H, quint, br, -CO-O-CH-), 4.16 (2H, t, -O-CH<sub>2</sub>-CH<sub>2</sub>-), 3.4 (2H, q, br, -CH<sub>2</sub>-CH<sub>2</sub>-NH-), 0.63–2.34 (m, br, CH<sub>3</sub>-C-CH<sub>2</sub>-, cholesterol) ppm.

<sup>13</sup>C NMR (75 MHz) in CDCl<sub>3</sub>:  $\delta$  = 167.3 (-C-CO-O-), 156.1 (-NH-CO-O-), 139.9 (-CH<sub>2</sub>-C=CH-), 136.2 (-CH<sub>2</sub>=C-CO-), 126.2 (CH<sub>2</sub>-C-CO-), 122.6 (-C=CH-CH<sub>2</sub>-), 74.6 (-O-CH-CH<sub>2</sub>-), 63.9 (-O-CH<sub>2</sub>-CH<sub>2</sub>-), 11.8–56.7 (-CH<sub>2</sub>-CH<sub>2</sub>-NH-, CH<sub>3</sub>-C-CH<sub>2</sub>-, Cholesterol) ppm.

FTIR:  $\nu^-$  = 3390, 2775–3000, 1634, and 1360 (cholesterol bands).

**Synthesis of P(NBoc-Glu-OtBu-MA)<sub>140</sub>-CTA via RAFT Polymerization:** In a reaction vessel, 564 mg NBoc-Glu-OtBu-MA ( $1.4 \times 10^{-3}$  mol, 150.0 equiv.), 0.15 mg AIBN ( $9.1 \times 10^{-7}$  mol, 0.1 equiv.), and 3.4 mg CDTA ( $9.1 \times 10^{-6}$  mol, 1.0 equiv.) were dissolved in 1.0 mL toluene and sealed with a rubber septum. The reaction mixture was deoxygenated with Ar for 30 min and subsequently placed in a preheated heating block and stirred at 70 °C for 24 h. The reaction was terminated by cooling to RT and purging air in. A sample was taken to determine the conversion via <sup>1</sup>H NMR spectroscopy in CDCl<sub>3</sub>. The crude polymer was diluted with DCM and precipitated in ice-cold *n*-hexane. After centrifugation (6000 rpm, 1 min), the supernatant was discarded, and the polymer was dried under reduced pressure to obtain the product as a yellow solid. SEC analysis can be found in Table 1.

**Synthesis of P(NBoc-Glu-OtBu-MA)<sub>140</sub>-b-(Chol-MA)<sub>10</sub>-CTA via RAFT Chain-Extension Polymerization:** In a reaction vessel, 20 mg Chol-MA ( $3.7 \times 10^{-5}$  mol, 20.0 equiv.), 0.06 mg AIBN ( $3.7 \times 10^{-7}$  mol, 0.2 equiv.), and 110 mg P(NBoc-Glu-OtBu-MA)<sub>140</sub>-CTA ( $1.9 \times 10^{-6}$  mol, 1.0 equiv.) were dissolved in 1.0 mL CHCl<sub>3</sub> and sealed with a rubber septum. The reaction mixture was deoxygenated with Ar for 20 min while cooling in an ice bath and subsequently placed in a preheated heating block and stirred at 70 °C for 24 h. The reaction was terminated by cooling to RT and purging air in. A sample was taken to determine the conversion via <sup>1</sup>H NMR spectroscopy in CDCl<sub>3</sub>. The crude polymer was precipitated in ice-cold *n*-hexane. After centrifugation (6000 rpm, 1 min), the supernatant was discarded, and the polymer was dried under reduced pressure to obtain the product as a yellow solid. SEC analysis can be found in Table 1 and Table S1 (Supporting Information).

**Removal of the Z-Group of P(NBoc-Glu-OtBu-MA)<sub>140</sub>-b-(Chol-MA)<sub>10</sub>-CTA Yielding P(NBoc-Glu-OtBu-MA)<sub>140</sub>-b-(Chol-MA)<sub>10</sub>:** The Z-group removal was conducted according to a literature procedure.<sup>[50]</sup> In a reaction vessel equipped with a stirrer bar, 100 mg P(NBoc-Glu-OtBu-MA)<sub>140</sub>-b-(Chol-MA)<sub>10</sub>-CTA ( $1.6 \times 10^{-6}$  mol, 1.0 equiv.), 5.3 mg AIBN ( $5.2 \times 10^{-5}$  mol, 20.0 equiv.) and 1.3 mg Luperox ( $1.3 \times 10^{-6}$  mol, 2.0 equiv.) were dissolved in 2 mL toluene. The vessel was sealed with a rubber septum and the reaction mixture was deoxygenated with Ar for 30 min. Subsequently, the vial was placed in a preheated heating block and heated to 80 °C for 2.5 h under continuous stirring. After cooling to RT, 1 mL of DCM was added and the crude mixture was precipitated in 40 mL ice-cold *n*-hexane, centrifuged (6000 rpm, 1 min) and the supernatant was discarded. The precipitation procedure was repeated thrice. The remaining solvent was evaporated under reduced pressure to obtain the product as a white solid.

ANOVA with Tukey's test. A) Cell growth in the presence of 6-MP-loaded NPs of a polymer concentration of 0.5 mg mL<sup>-1</sup>. Dashed line represents the threshold for acute cytotoxicity (79% of NC) according to ISO-10993-5.<sup>[44]</sup> B) Relative cell populations on day 3 for the drug concentration of 25 µg mL<sup>-1</sup>, corresponding to 0.5 mg mL<sup>-1</sup> polymer (0 and 5 wt.% 6-MP), 0.25 mg mL<sup>-1</sup> polymer (10 wt.% 6-MP) and 0.13 mg mL<sup>-1</sup> polymer (20 wt.% 6-MP). Significances are relative to the corresponding control. Dashed line represents relative cell viability at day 0 (100%). C) Relative cell populations on day 3 at either the same concentration of polymer (0.5 mg mL<sup>-1</sup>) or 6-MP (25 µg mL<sup>-1</sup>). Significances are relative to NPs with 0 wt.% 6-MP at a polymer concentration of 0.5 mg mL<sup>-1</sup>.

**Acidic Deprotection of P(NBoc-Glu-OtBu-MA)<sub>140</sub>-b-(Chol-MA)<sub>10</sub> Yielding P(Glu-OH-MA)<sub>140</sub>-b-(Chol-MA)<sub>10</sub>:** In a reaction vessel, 50 mg of P(NBoc-Glu-OtBu-MA)<sub>140</sub>-b-(Chol-MA)<sub>10</sub> were dissolved in 1 mL trifluoroacetic acid, and the reaction was stirred at room temperature for 1 h.

Subsequently, the reaction mixture was diluted with 4 mL MeOH and the polymer was precipitated in a mixture of 40 mL ice-cold diethyl ether and 5 mL ice-cold *n*-hexane. Then, the suspension was centrifuged (6 000 rpm, 1 min) and the supernatant was discarded. The polymer was re-dissolved in diH<sub>2</sub>O and lyophilized to obtain the product as a white powder.

The success of the deprotection of the polymer was analyzed by <sup>1</sup>H NMR in D<sub>2</sub>O, showing the disappearance of the Boc, respectively *t*Bu, signal around  $\delta = 1.4$  ppm.

**Thin-Film Assembly:** The self-assembly of block copolymers was conducted by the thin-film hydration method.<sup>[40]</sup> In a 4 mL glass vial, 1 mg of block copolymer (and the respective amount of 6-MP) was dissolved in 1 mL of methanol. Then, the solvent was completely removed under a mild stream of airflow while shaking (100 rpm) overnight. Subsequently, 1 mL of DPBS was added while shaking (100 rpm) to acquire (6-MP-loaded) polymer NPs (1 mg mL<sup>-1</sup> in DPBS). The weight percentages (wt.%) of 6-MP refer to the theoretical amount encapsulated.

**Biological Evaluation—Cell Culture:** MDA-MB-231 cells were grown in DMEM/F12 supplemented with 10% (v/v) FBS, 100 U mL<sup>-1</sup> penicillin, and 100  $\mu$ g mL<sup>-1</sup> streptomycin.

**Biological Evaluation—Cell Viability:** Cells were cultured as described above. For the cell viability assay, cells (10<sup>4</sup> per well) were seeded in 96-well plates and allowed to adhere overnight. No cells were seeded in the outer wells. The media was subsequently removed and replaced by fresh polymer-containing media. Then, the cells were incubated at 37 °C for an additional 24 h. After that, the media was removed, the cells were washed with 100  $\mu$ L DPBS, and then fresh media containing the thiazolyl blue tetrazolium bromide (MTT) (concentration: 1 mg mL<sup>-1</sup>) was added (100  $\mu$ L per well). Note: MTT (50 mg) was dissolved in 10 mL of sterile DPBS, filtered (membrane, 0.22  $\mu$ m), and 1 to 5 diluted in culture medium prior to use in this assay. After incubation for 3 h at 37 °C, 50  $\mu$ L of DMSO was added to each well and the plates were gently shaken in the dark for 1 h to dissolve the formazan crystals. Quantification was done by measuring the absorbance at  $\lambda = 590$  nm using a microplate reader. Untreated cells on the same plate served as negative control (100% viability), cells treated with 20% DMSO as positive control (0% viability), and wells without cells as background. Experiments were performed in triplicates.

$$\%Cell\ viability = \frac{Abs.\ sample - Abs.\ background}{Abs.\ negative\ control - Abs.\ background} \cdot 100 \quad (4)$$

**Biological Evaluation—Cell Growth Inhibition Assays:** Cell growth inhibition assays were conducted as previously reported.<sup>[51]</sup> The following alterations were made to the MTT protocol described in ref. 51. Cells were seeded at a density of 3 × 10<sup>3</sup> cells per well. One plate was used for each time point. Media was changed daily. After the indicated time points (0, 1, 2, or 3 days), (polymer-containing) cell medium was removed, and cells were gently washed with 100  $\mu$ L of DPBS before the addition of fresh medium containing the MTT reagent as described in ref. [51] and incubated for 3 h at 37 °C. The relative cell viability was determined by Equations 5 and 6.

$$Cell\ growth = \frac{(absorbance\ (sample\ or\ control) - absorbance\ (blank))}{absorbance\ (blank)} \quad (5)$$

$$Relative\ cell\ growth = \frac{cell\ growth\ (sample\ or\ control\ day\ n)}{cell\ growth\ (control\ day\ 0)} \quad (6)$$

**Statistical Analysis:** All data plotted with error bars were expressed as means with standard deviation. *p*-Values were generated by analyzing data with a one-way ANOVA and Turkey test using OriginLab.

**Computations:** The machine learning predictors of the Polymer Genome project were used to predict the density of the block copolymers.

These predictors employed advanced multi-task neural networks that simultaneously predicted multiple polymer properties and leveraged data correlations to enhance their accuracy. The predictors were trained and evaluated on a large dataset containing a variety of polymer properties. The partition coefficients of the block copolymers were computed using the cheminformatics tool RDKit which implemented the method described by Wildman and Crippen.

## Supporting Information

Supporting Information is available from the Wiley Online Library or from the author.

## Acknowledgements

M.N.L. acknowledges financial support from the “Fonds der Chemischen Industrie (FCI) im Verband der Chemischen Industrie e.V. (VCI)”. R.H. and B.D.G. acknowledge continuous financial support from the Research Foundation – Flanders (FWO) and Ghent University (BOF). The authors thank Rika Schneider for assistance with size-exclusion chromatography measurements.

Open access funding enabled and organized by Projekt DEAL.

## Conflict of Interest

The authors declare no conflict of interest.

## Author Contributions

M.N.L. did conceptualization, methodology, formal analysis, investigation, data curation, writing – original draft, visualization, supervision, project administration, and funding acquisition. C.K. contributed to software, data curation, visualization, and writing – review and editing. J.D.B. was involved in the investigation, data curation, visualization, and writing – review and editing. B.G.D.G. participated in methodology and writing – review and editing. R.H.’s contributions encompassed conceptualization, methodology, supervision, and writing – review and editing, along with funding acquisition.

## Data Availability Statement

The data that support the findings of this study are available from the corresponding author upon reasonable request.

## Keywords

6-mercaptopurine, cholesterol, RAFT polymerization, self-assembly, zwitterionic polymers

Received: June 23, 2023

Revised: July 26, 2023

Published online:

- [1] a) C. Englert, J. C. Brendel, T. C. Majdanski, T. Yildirim, S. Schubert, M. Gottschaldt, N. Windhab, U. S. Schubert, *Prog. Polym. Sci.* **2018**, *87*, 107; b) R. Haag, F. Kratz, *Angew. Chem., Int. Ed.* **2006**, *45*, 1198.
- [2] a) R. Duncan, R. Gaspar, *Mol. Pharmaceutics* **2011**, *8*, 2101; b) R. Duncan, M. J. Vicent, *Adv. Drug Delivery Rev.* **2013**, *65*, 60; c) F. Greco, M. J. Vicent, *Adv. Drug Delivery Rev.* **2009**, *61*, 1203; d) K. Greish, J. Fang, T. Inutsuka, A. Nagamitsu, H. Maeda, *Clin. Pharmacokinet.* **2003**, *42*, 1089.

- [3] Z. He, X. Wan, A. Schulz, H. Bludau, M. A. Dobrovolskaia, S. T. Stern, S. A. Montgomery, H. Yuan, Z. Li, D. Alakhova, M. Sokolsky, D. B. Darr, C. M. Perou, R. Jordan, R. Luxenhofer, A. V. Kabanov, *Biomaterials* **2016**, *101*, 296.
- [4] R. Luxenhofer, Y. Han, A. Schulz, J. Tong, Z. He, A. V. Kabanov, R. Jordan, *Macromol. Rapid Commun.* **2012**, *33*, 1613.
- [5] N. Bertrand, J. Wu, X. Xu, N. Kamaly, O. C. Farokhzad, *Adv. Drug Delivery Rev.* **2014**, *66*, 2.
- [6] P. L. Turecek, M. J. Bossard, F. Schoetens, I. A. Ivens, *J. Pharm. Sci.* **2016**, *105*, 460.
- [7] a) R. Hoogenboom, *Eur. Polym. J.* **2022**, *179*, 111521; b) S. Nemati Mahand, S. Aliakbarzadeh, A. Moghaddam, A. Salehi Moghaddam, B. Kruppke, M. Nasrollahzadeh, H. A. Khonakdar, *Eur. Polym. J.* **2022**, *178*, 111484.
- [8] P. Chytil, L. Kostka, T. Etrych, *J Pers Med* **2021**, *11*, 115.
- [9] a) M. Barz, R. Luxenhofer, R. Zentel, M. J. Vicent, *Polym. Chem.* **2011**, *2*, 1900; b) H. Hatakeyama, H. Akita, H. Harashima, *Biol. Pharm. Bull.* **2013**, *36*, 892.
- [10] Z. Amoozgar, Y. Yeo, *Wiley Interdiscip. Rev.: Nanomed. Nanobiotechnol.* **2012**, *4*, 219.
- [11] Z. Zhang, S. Chen, S. Jiang, *Biomacromolecules* **2006**, *7*, 3311.
- [12] a) L. D. Blackman, P. A. Gunatillake, P. Cass, K. E. S. Locock, *Chem. Soc. Rev.* **2019**, *48*, 757; b) B. Zhou, J. Li, B. Lu, W. Wu, L. Zhang, J. u Liang, J. Yi, X. Li, *Front. Mater. Sci.* **2020**, *14*, 402.
- [13] H. S. Choi, W. Liu, F. Liu, K. Nasr, P. Misra, M. G. Bawendi, J. V. Frangioni, *Nat. Nanotechnol.* **2010**, *5*, 42.
- [14] a) S. Fujii, K. Sakurai, *Biomacromolecules* **2022**, *23*, 3968; b) S. Fujii, S. Takano, K. Nakazawa, K. Sakurai, *Biomacromolecules* **2022**, *23*, 2846; c) Yi Li, H. Yu Yang, T. Thambi, J.-H. Park, D. S. Lee, *Biomaterials* **2019**, *217*, 119299; d) I. Theodorou, P. Anilkumar, B. Lelandais, D. Clarisse, A. Doerflinger, E. Gravel, F. Ducongé, E. Doris, *Chem. Commun.* **2015**, *51*, 14937.
- [15] A. Laschewsky, *Polymers* **2014**, *6*, 1544.
- [16] S. Takano, K. Sakurai, S. Fujii, *Polym. Chem.* **2021**, *12*, 6083.
- [17] a) M. N. Leiske, Z. A. I. Mazrad, A. Zelcak, K. Wahi, T. P. Davis, J. A. Mccarroll, J. Holst, K. Kempe, *Biomacromolecules* **2022**, *23*, 2374; b) M. N. Leiske, B. G. De Geest, R. Hoogenboom, *Bioact Mater* **2023**, *24*, 524.
- [18] P. L. Yeagle, *Biochim. Biophys. Acta – Biomembr.* **1985**, *822*, 267.
- [19] a) P. Sellaturay, S. Nasser, S. Islam, P. Gurugama, P. W. Ewan, *Clin. Exp. Allergy* **2021**, *51*, 861; b) K. A. Risma, *Curr. Opin. Pediatr.* **2021**, *33*, 610.
- [20] K. Shoji, Y. Nakajima, E. Ueda, M. Takeda, *Polym J* **1985**, *17*, 997.
- [21] S.-J. He, Y. Zhang, Z.-H. Cui, Y.-Z. Tao, B.-L. Zhang, *Eur. Polym. J.* **2009**, *45*, 2395.
- [22] J. A. Nelson, J. W. Carpenter, L. M. Rose, D. J. Adamson, *Cancer Res.* **1975**, *35*, 2872.
- [23] R. Kamojjala, B. Bostrom, *J Pediatr Hematol Oncol* **2021**, *43*, 95.
- [24] a) J. Yao, J.-M. Chen, Y.-i.-B. o Xu, T.-B.-u Lu, *Cryst. Growth Des.* **2014**, *14*, 5019; b) A. H. Ahmed, Y. A. E. Badr, *Arab J. Nucl. Sci. Appl.* **2018**, *51*, 181.
- [25] M. Zacchigna, F. Cateni, G. Di Luca, S. Drioli, *Bioorganic Med. Chem. Lett.* **2007**, *17*, 6607.
- [26] a) L. Chen, G. Pilia, R. Batra, T. D. Huan, C. Kim, C. Kuenneth, R. Ramprasad, *Mater Sci Eng R Rep* **2021**, *144*, 100595; b) D. J. Audus, J. J. De Pablo, *ACS Macro Lett.* **2017**, *6*, 1078.
- [27] a) C. Kuenneth, J. Lalonde, B. L. Marrone, C. N. Iverson, R. Ramprasad, G. Pilia, *Commun. Mater.* **2022**, *3*, 96; b) C. Kuenneth, A. C. Rajan, H. Tran, L. Chen, C. Kim, R. Ramprasad, *Patterns* **2021**, *2*, 100238.
- [28] H. Doan Tran, C. Kim, L. Chen, A. Chandrasekaran, R. Batra, S. Venkatram, D. Kamal, J. P. Lightstone, R. Gurnani, P. Shetty, M. Ramprasad, J. Laws, M. Shelton, R. Ramprasad, *J. Appl. Phys.* **2020**, *128*, 171104.
- [29] S. A. Wildman, G. M. Crippen, *J. Chem. Inf. Model.* **1999**, *39*, 868.
- [30] Y.-K. Lee, K. Onimura, H. Tsutsumi, T. Oishi, *J. Polym. Sci., Part A: Polym. Chem.* **2000**, *38*, 4315.
- [31] a) U. Domańska, C. Klofutar, Š. Paljk, *Fluid Phase Equilib.* **1994**, *97*, 191; b) G. L. Flynn, Y. Shah, S. Prakongpan, K. H. Kwan, W. I. Higuchi, A. F. Hofmann, *J. Pharm. Sci.* **1979**, *68*, 1090; c) M. M. Stevens, A. R. Honerkamp-Smith, S. L. Keller, *Soft Matter* **2010**, *6*, 5882.
- [32] D. T. Gentekos, R. J. Sifri, B. P. Fors, *Nat. Rev. Mater.* **2019**, *4*, 761.
- [33] R. Mahon, Y. Balogun, G. Oluyemi, J. Njuguna, *SN Appl Sci* **2019**, *2*, 117.
- [34] M. A. Moharram, M. G. Khafagi, *J. Appl. Polym. Sci.* **2006**, *102*, 4049.
- [35] I. C. Mcneill, S. M. T. Sadeghi, *Polym. Degrad. Stab.* **1990**, *29*, 233.
- [36] S. G. Roy, K. Bauri, S. Pal, P. De, *Polym. Chem.* **2014**, *5*, 3624.
- [37] M. Nandi, B. Maiti, S. Banerjee, P. De, *J. Polym. Sci., Part A: Polym. Chem.* **2019**, *57*, 511.
- [38] R. Bilbao, J. F. Mastral, J. Ceamanos, M. E. Aldea, *J. Anal. Appl. Pyrolysis* **1996**, *37*, 69.
- [39] A. M. Beagan, *Int. J. Environ. Anal. Chem.* **2023**, *103*, 947.
- [40] Z. A. I. Mazrad, B. Schelle, J. A. Nicolazzo, M. N. Leiske, K. Kempe, *Biomacromolecules* **2021**, *22*, 4618.
- [41] P. J. Flory, *J. Am. Chem. Soc.* **1940**, *62*, 1057.
- [42] D. E. Discher, F. Ahmed, *Annu. Rev. Biomed. Eng.* **2006**, *8*, 323.
- [43] M. Swain, S. Turk, A. Saveliev, A. Vaucher, M. Wójcikowski, I. Take, D. Probst, K. Ujihara, V. F. Scaffani, G. Godin, J. Lehtivarjo, A. Pahl, R. Walker, F. Berenger, jasondbiggs, strets123, *Zenodo* **2023**, Rdkit/rdkit: 2023\_03\_2 (q1 2023) release. <https://doi.org/10.5281/zenodo.8053810>.
- [44] I. O. F. Standardization, *Iso-10993-5. Biological evaluation of medical devices. Part 5: Tests for cytotoxicity: In vitro methods*, The Organization Geneva, **1992**.
- [45] C. M. Galmarini, J. R. Mackey, C. Dumontet, *Lancet Oncol.* **2002**, *3*, 415.
- [46] T. J. Kochel, J. C. Reader, X. Ma, N. Kundu, A. M. Fulton, *OncoTargets Ther.* **2017**, *8*, 6540.
- [47] L. Lennard, *Eur J Clin Pharmacol* **1992**, *43*, 329.
- [48] M. Ghorbani, H. Hamishehkar, *Mater. Sci. Eng. C* **2018**, *92*, 599.
- [49] V. Kottisch, D. T. Gentekos, B. P. Fors, *ACS Macro Lett.* **2016**, *5*, 796.
- [50] M. Chen, G. Moad, E. Rizzardo, *J. Polym. Sci., Part A: Polym. Chem.* **2009**, *47*, 6704.
- [51] Z. Jiang, H. Liu, H. He, N. Yadava, J. J. Chambers, S. Thayumanavan, *Bioconjugate Chem.* **2020**, *31*, 1344.